Results in Chemistry 4 (2022) 100283

Contents lists available at ScienceDirect

Results in Chemistry

journal homepage: www.sciencedirect.com/journal/results-in-chemistry

Study of SO_2 into nanoporous silica Y Zeolite: Molecular dynamics simulation

Yalda Sabahi [a], Mohammad Razmkhah [b], Fatemeh Moosavi [a,*]

[a] Department of Chemistry, Faculty of Science, Ferdowsi University of Mashhad, Mashhad 9177948974, Iran
[b] Department of Chemical Engineering, Ferdowsi University of Mashhad, Mashhad 9177948944, Iran

ARTICLE INFO

Keywords:
Porous Y zeolite
Sulfur dioxide
Diffusion
Fickian behavior
Potential of mean force

ABSTRACT

The dynamic, structure, and thermodynamic properties of sulfur dioxide guest gas inside nanoporous fixed silica Y zeolite were studied by molecular dynamics simulation at different loadings of SO_2 per unit cell and within a range of temperature. At loading 20, greater deviation from Fickian behavior is observed. Generally, self-diffusion coefficient increases with temperature. The activation energy for diffusion follows a decreasing trend by loading increase, except at loading 20, which shows an increase in activation energy. The velocity autocorrelation function demonstrates oscillating behavior and cage effect decrease with temperature. From the radial distribution function (RDF) between gas and zeolite framework, it is found that the first layer around the central atom at a low temperature is established more easily and the first peak of the RDF appears at a short distance with more intensity. The interaction between S and Si atoms was examined by the potential of mean force that is independent of loading. The results indicate that SO_2 is able to disperse homogeneously into the zeolite at all concentrations and temperatures without much perturbation.

1. Introduction

Sulfur dioxide (SO_2) is an acidic, colorless, nonflammable, and toxic gas with a pungent and irritating smell [1–4]. SO_2 emission deriving from fossil fuel combustion processes in thermal power plants, petroleum refinery or on-road vehicles created serious environmental concerns so that its control remains a challenging problem [5–7]. In 2013, Deng et al. [8] have reported that more than 98% of SO_2 emission is mainly generated from the combustion of fossil fuels and considering over 85% of the energy demand due to the progressive industrialization of the world is currently supplied by fossil fuels; this problem has emerged as a serious global issue. SO_2 is directly responsible for the acid rain, air pollution, and health problems. In addition, it is harmful to human health and the ecosystem as well as ozone layer depletion in the stratosphere [5,9–11]. On the other hand, SO_2 has applications in the chemical industry; for example, not only is widely used as a food preservative for dried fruits [1] but also is fundamental in producing sulfuric acid [12].

Considering these mutual properties of SO_2, its removal as well as storing has attracted academic and industrial scientists to explore various techniques. Some technologies are often multistep, complex, and costly processes [8,13,14]. Thus, many attempts have been made to find a single-step process and suitable method for removing and storing SO_2. One of these processes is adsorption of SO_2 in nonoporous solids or on nanomaterials that have attracted increasing attention for significant advantages over other approaches such as, the minimum energy requirements for the regeneration of the adsorbent, relatively simple design compared to a chemical reactor and minimum waste disposal problems [13,15].

Non-regenerative and regenerative solid adsorbents are applied in controlling emissions of SO_2 acidic gas. The former examples are CaO and MgO with major drawback of being blocked due to the sorption process by sulphate layers. The other type, which has the ability for the continuous regeneration such as, zeolites, metal-organic frameworks (MOFs), zeolitic imidazolate frameworks (ZIFs), silica gel, and charcoal, is used widely for acidic gas removal by adsorption [16–19].

In this series of solid adsorbents, zeolites are as one of the safe, effective, and affordable ones for the capture and storage of SO_2 from flue gas [8,9,13,19,20]. Zeolites are crystalline microporous aluminosilicates containing channels and cavities with molecular dimensions [21–24]. Because of high thermal and chemical stabilities, adjustable composition, low density, and high void volume, zeolites have been

* Corresponding author.
E-mail address: moosavibaigi@um.ac.ir (F. Moosavi).

https://doi.org/10.1016/j.rechem.2022.100283
Received 21 September 2021; Accepted 5 January 2022
Available online 10 January 2022

Table 1
The partial atomic charges and LJ parameters used for atoms of the zeolite framework and SO_2 gas in the MD simulations (O: oxygen atom of Y zeolite and O_S: oxygen atom of SO_2) [45,46].

Atom	q/e	ε/kcal.mol^{-1}	σ/Å
Si	1.100	0.162	3.962
O	−0.550	0.058	3.062
S	0.402	0.376	3.410
O_S	−0.201	0.117	3.198

widely used to remove various types of pollutants from the environment [20,22,25,26]. Classification of zeolites is based on their composition, pore size, pore network topology, and channel system [27]. FAU is a type of zeolite family named as molecular sieve for its greater pores that can store more amount of gas. Due to regular structure and high internal surface, FAU zeolites have been broadly used in practical applications of adsorption and separation in the process of producing clean fuels [28]. The FAU zeolite has large cages connected by narrow window; furthermore, it has the minimum resistance to mass transfer due to the wide pore distribution and large pore volume [29]. The simplest type of FAU is SiO_2 and the presence of different metal ions leads to variety in

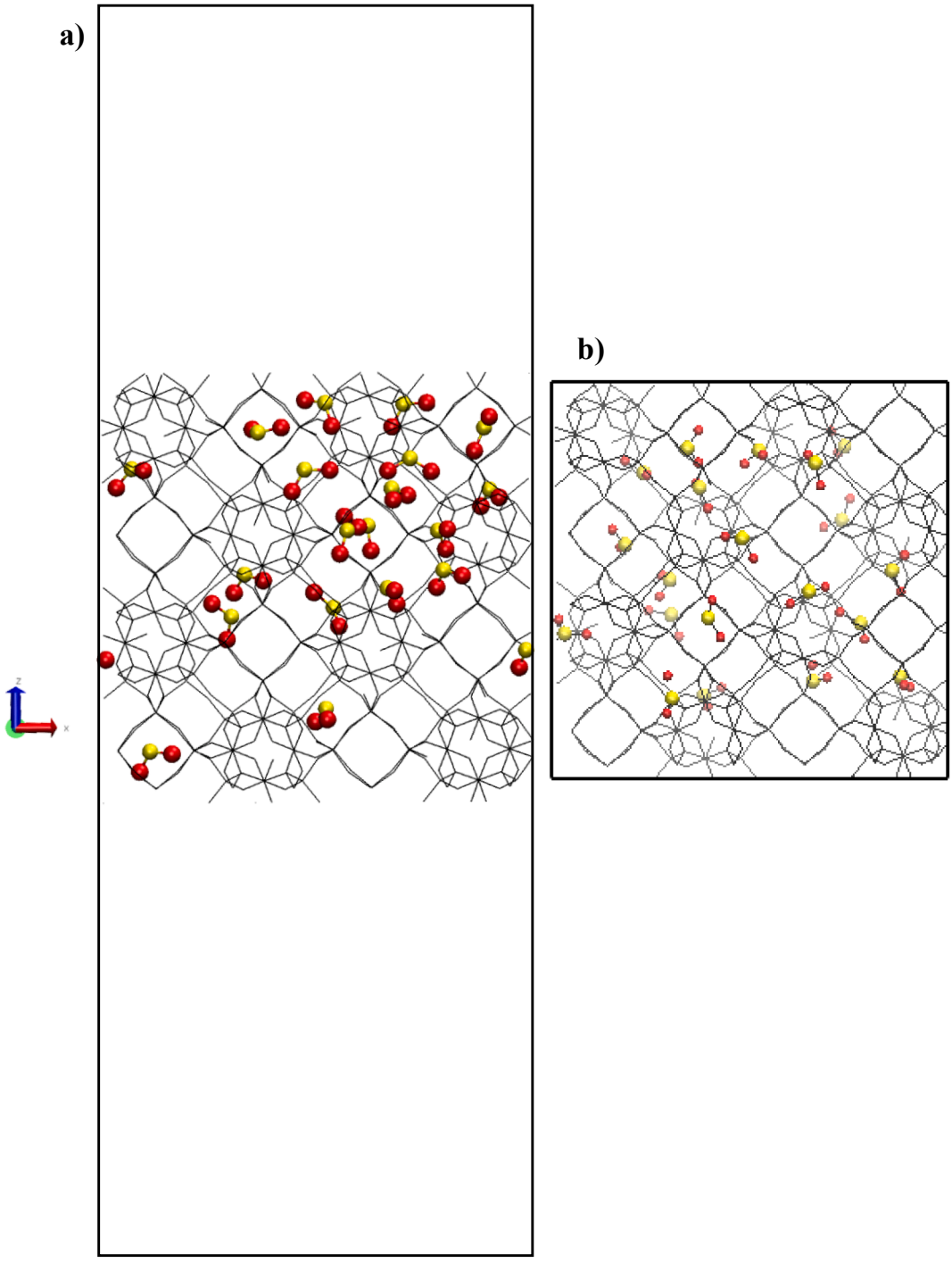

Fig. 1. End-of-simulation snapshot of 20 SO_2 molecules inside Y zeolite pores at 300 K. (a) rectangular cube box and (b) cubic box.

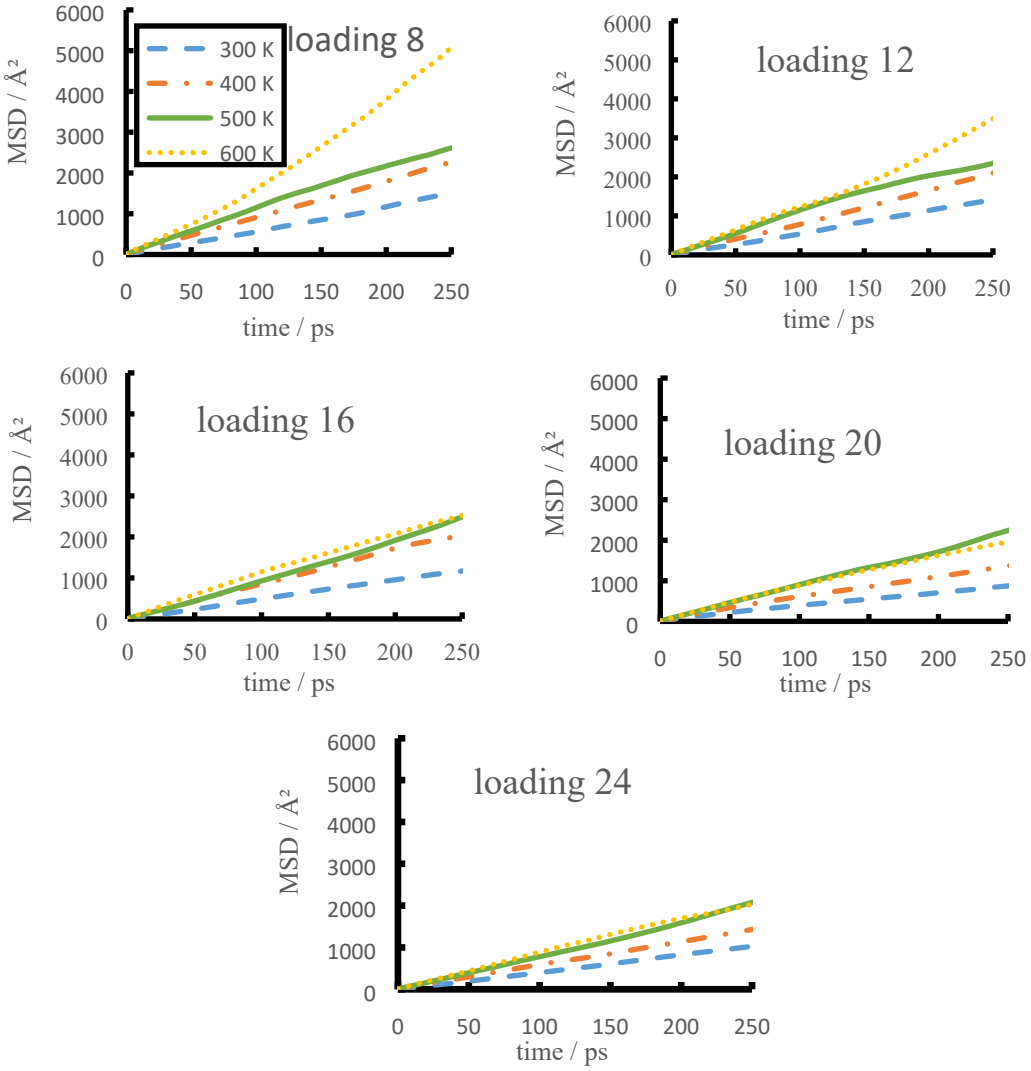

Fig. 2. The effect of temperature on the computed center of mass MSD of SO_2 within pores of silica Y zeolite from simulations at different loadings.

structure and application. Molecular classical simulation techniques, which consist of the Monte Carlo (MC) and molecular dynamics (MD) methods, have become powerful tools to study the static and dynamic properties of molecular systems [30–34]. Experiments include disadvantages, such as, environmental pollution and high cost that limit their application; from the other side of view, the molecular simulations do not have these weaknesses. Besides, the simulation provides a molecular perspective and is a method to study the microscopic details of the diffusion process.

Accordingly, people have performed different studies helping molecular simulation to remove or adsorb various gases by FAU zeolite. In 1992, Santikary et al. [30] have examined temperature and concentration dependence of Xenon sorption in Na-Y zeolite. They have concluded that the activation energy of diffusion coefficient is 4.1 $kJ.mol^{-1}$ and crossing from ballistic to diffusive behavior was observed. Mizukami et al. [35], in 2001, have carried out MD calculations for the separation of CO_2 from a mixture of CO_2/N_2 by zeolite with a Si/Al = 2.47 ratio with an exciting result that nitrogen is not adsorbed on zeolite. Kamat et al. [36] have investigated the adsorption and diffusion behavior of methane in Na-Y zeolite by MD simulation at 5 temperatures and different loadings. An acceptable agreement between MD results and their analytical theory was obtained. In 2008, a research has been performed on the removal of hydrogen sulfide and its competitive adsorption toward methane and carbon dioxide by zeolites MFI (dealumined), Na-Y (Si/Al = 1) and LTA (Si/Al = 1) with Coupled Grand Canonical-Canonical Monte Carlo and MD simulation techniques. It was found that Na-Y zeolite is the best option for the removal of hydrogen sulfide [32]. Na-X and Na-Y Faujasite systems were applied to understand CO_2 adsorption mechanism [37]; water diffusion in zeolites Na-X and Na-Y was investigated theoretically and experimentally at different temperatures and loadings [38]. In addition, Deroche et al. [39] have studied self-diffusion coefficients and adsorption isotherms of pure methane and its binary mixture with CO_2 in Na-Y zeolite at 200 K by combining an experimental quasi-elastic neutron scattering (QENS) technique and classical MD simulations. The study demonstrated that Na-Y has more ability to adsorb CH_4 while CH_4 self-diffusion coefficient decreases when CO_2 loading increases. In 2014, Thang et al. [40] have reported a spectroscopic, calorimetric, and theoretical study on the effect of composition on equilibrium CO_2 adsorption in M−FAU (M = Li, Na, and K). In 2014, Zhang et al. [34] have investigated the adsorption of CO_2 and CH_4 in Na-Y and Na-X zeolites by grand-canonical MC (GCMC) simulations. The results of adsorption isotherms were fitted by Langmuir and Toth models. In 2015, Lima et al. [41] have investigated the adsorption of a 15:85 (CO_2 : N_2) mixture on Na-X zeolite impregnated with monoethanolamine (MEA) by MC simulation. They have understood that CO_2 selectivity is higher than N_2 by the goal adsorbent. Furthermore, MEA concentrations higher than 12 wt% prevented the adsorption of CO_2 molecules. In 2015, Sun et al. [29] have evaluated the

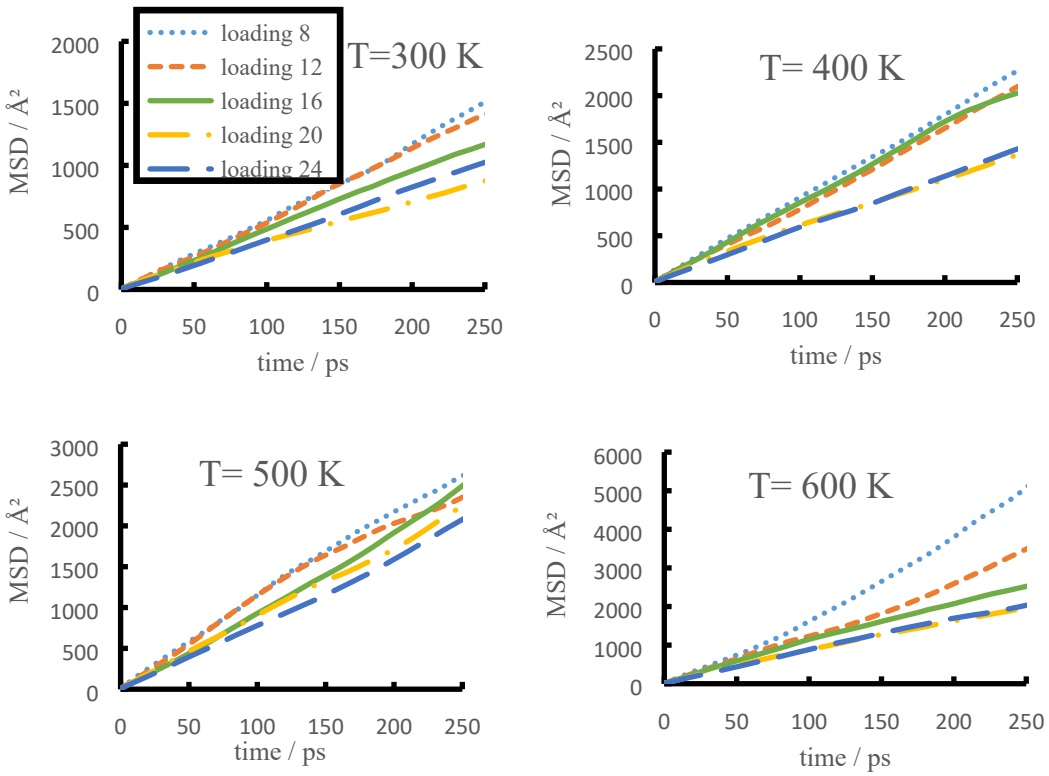

Fig. 3. The effect of loading (molecules per unit cell) changes on the computed center of mass guest molecule MSD within the pores of silica Y zeolite from simulations at different temperatures.

Table 2
The computed self-diffusion coefficient of SO_2 in silica Y zeolite, uncertainty values are shown in parentheses, β values at different loadings and temperatures, and diffusion activation energies.

T (K)	8 mol/u.c.		12 mol/u.c.		16 mol/u.c.		20 mol/u.c.		24 mol/u.c.	
	β	$D \times 10^9$ ($m^2.s^{-1}$)	β	$D \times 10^9$ ($m^2.s^{-1}$)	β	$D \times 10^9$ ($m^2.s^{-1}$)	β	$D \times 10^9$ ($m^2.s^{-1}$)	β	$D \times 10^9$ ($m^2.s^{-1}$)
300	0.98	9.95 (± 0.29)	0.98	9.55 (± 0.14)	0.97	7.90 (± 0.19)	0.85	5.56 (± 0.12)	0.98	6.92 (± 0.13)
400	0.95	14.90 (± 0.23)	0.96	13.91 (± 0.24)	0.96	13.86 (± 0.26)	0.89	8.76 (± 0.27)	0.94	9.38 (± 0.16)
500	0.93	17.41 (± 0.40)	0.95	15.83 (± 0.54)	1.00	16.44 (± 0.31)	0.95	14.46 (± 0.25)	0.97	13.57 (± 0.35)
600	1.06	34.12 (± 0.60)	0.97	22.37 (± 0.63)	0.92	16.55 (± 0.28)	0.90	12.84 (± 0.32)	0.94	13.61 (± 0.35)
E_{act} (kJ.mol^{-1})	5.44		3.93		3.84		4.72		3.66	

diffusion of N_2 , O_2 , H_2S , and SO_2 gases in MFI and 4A zeolites by MD simulation. At high temperatures and loadings, the diffusion coefficient of SO_2 is lower than the other gases concluding that SO_2 has the highest adsorption. In MFI, the diffusion coefficient of SO_2 increases uniformly with increasing temperature and decreases with increasing loading, but in 4A it does not change with increasing loading. Asl et al. [42] have simulated the decryption of bi and tri aromatics behavior with Na-X zeolite. In 2017, Kowsari and Naderlou [17] have taken under consideration the diffusion of H_2 molecules through fixed Li-LSX zeolite by MD simulation. They have shown that at a loading and temperature range, the order of self-diffusion coefficient of H_2 guest was 10^{-9} up to $10^{-7} m^2 . s^{-1}$ and the activation energy was reported to be ~ 2 kcal.mol^{-1}. However, the absorption and solubility of SO_2 toxic gas in glycol monomethyl ether and dimethyl sulfoxide system was a spontaneous process and decreased with the increasing temperatures; in addition, a high molecular ordering was observed because of intermolecular interactions between the solvent and the gas [43].

Considering that in our best knowledge, the investigation of the adsorption or removal of SO_2 by silica Y zeolite has not been carried out with molecular perspectives, the present study evaluates the diffusion of SO_2 gas in silica Y zeolite cages by MD simulation. Moreover, the effect of temperature and gas loading is studied on the SO_2 diffusion. A more detailed investigation of gas in the zeolite cages is given by studying radial distribution function (RDF) as well as velocity autocorrelation function (VAF). However, the study evaluates the behavior of gas in the cage in detail from the molecular viewpoint that has not been considered previously.

2. Computational methods

Primary structure of cubic unit cell ($Fd\ \bar{3}\ m$) of the silica Y zeolite with [$Si_{192}O_{384}$] formula unit and $a = 24.345$ Å was created on the base of the crystallographic information file taken from database of zeolite structures [44]. Here, the structure of the Y zeolite framework during the simulation was considered fixed. The 12-member windows of the Y zeolite have a diameter of 7.4 Å. Considering the kinetic diameter SO_2 (3.6 Å), the zeolite framework was fixed. It does not seem to have a significant impact on the magnitude or the trend of the diffusivity. Furthermore, based on the previous studies [16,29,39], it can be received that flexibility has no significant effect on the diffusion of small gas molecules at low loading. The Lennard-Jones (LJ) potential was used for the van der Waals (vdW) pair interactions. Partial atomic charges

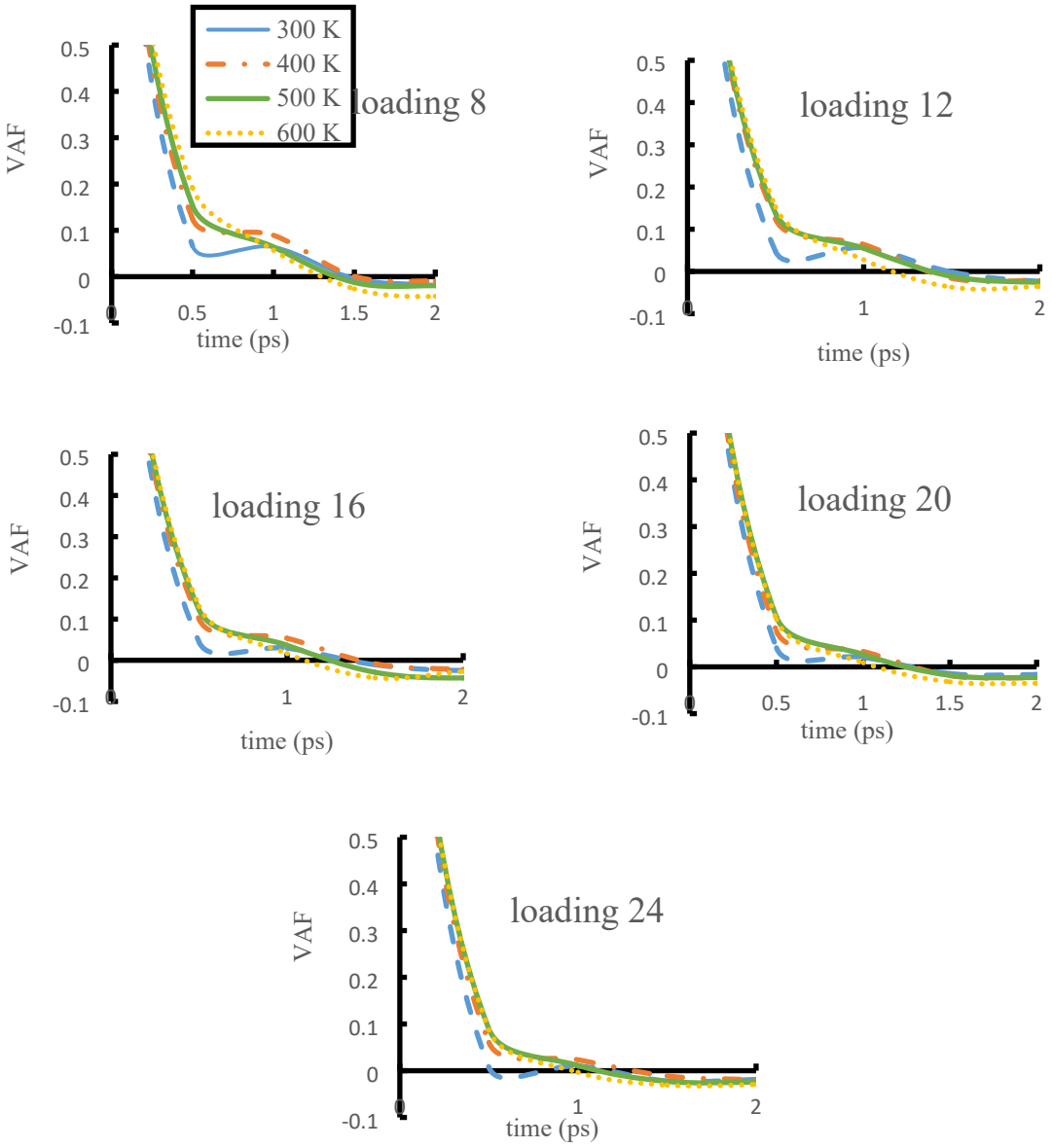

Fig. 4. Short time behavior of the velocity autocorrelation functions of S atom from simulations at different loadings and temperatures.

and LJ parameters were taken from Nicholas et al. [45] and Palmer et al. [46]. SO_2 molecule was considered rigid with bond length 1.431 Å and bond angle of O-S-O is equal to 119° [3]. All the applied parameters are summarized in Table 1.

The LJ parameters between different atom types were generated from the Lorenz-Berthelot mixing rules, $\varepsilon_{ij} = \sqrt{\varepsilon_{ii}\varepsilon_{jj}}$ and $\sigma_{ij} = \frac{1}{2}(\sigma_{ii} + \sigma_{jj})$ [20,46]. All simulations have been done using DL_POLY_2.17 [47] program on a Linux workstation. One unit-cell of FAU was used as the simulation box because size effect was not seen for the system of concern [28]. Moreover, periodic boundary conditions were applied. The behavior of SO_2 was investigated for loadings of 8, 12, 16, 20, and 24 molecules per unit cell (mol/u.c.). The MD simulations were performed at 300, 400, 500, and 600 K; the initial structure was equilibrated for a time of 2000 ps. The length of MD runs for data production is 1000 ps. Time step in all simulations was 1.0 fs and cut-off radius of 12 Å was considered. The simulations were performed in NVT to equilibrate the system and in NVE ensemble for production step by rescaling the velocities to control the desired temperature. Equations of motion were integrated with leapfrog algorithm. The Ewald summation method was used to calculate long-range electrostatic interactions. First, a simulation was carried out with a rectangular cube box. So that SO_2 molecules were located in the empty space above the box. 2 ns was taken to allow SO_2 molecules to enter the zeolite cages. Then, SO_2 molecules that remained outside the zeolite were removed, the box was converted to a cubic box and it was used for the SO_2 molecules diffusion into the cube cages as a new simulation box. The simulation was repeated for this system as above mentioned. As a typical sample, Fig. 1 shows a snapshot of simulation box at the final time of simulation for loading 20 at 300 K at both stages of MD simulation.

Self-diffusion coefficient was calculated from the long-time limit of MSD using well-known Einstein relation,

$$D_i = \frac{1}{6}\lim_{t\to\infty}\frac{d}{dt}\left\langle \left[r_i^c(t) - r_i^c(0)\right]^2 \right\rangle \quad (1)$$

where D_i is the self-diffusion coefficient, $r_i^c(t)$ and $r_i^c(0)$ denote the position vector of the center of mass of molecule at time t and 0, respectively [20,39,48,49].

To determine the diffusion mechanism using the mean squared displacement (MSD), β factor was introduced which is defined as

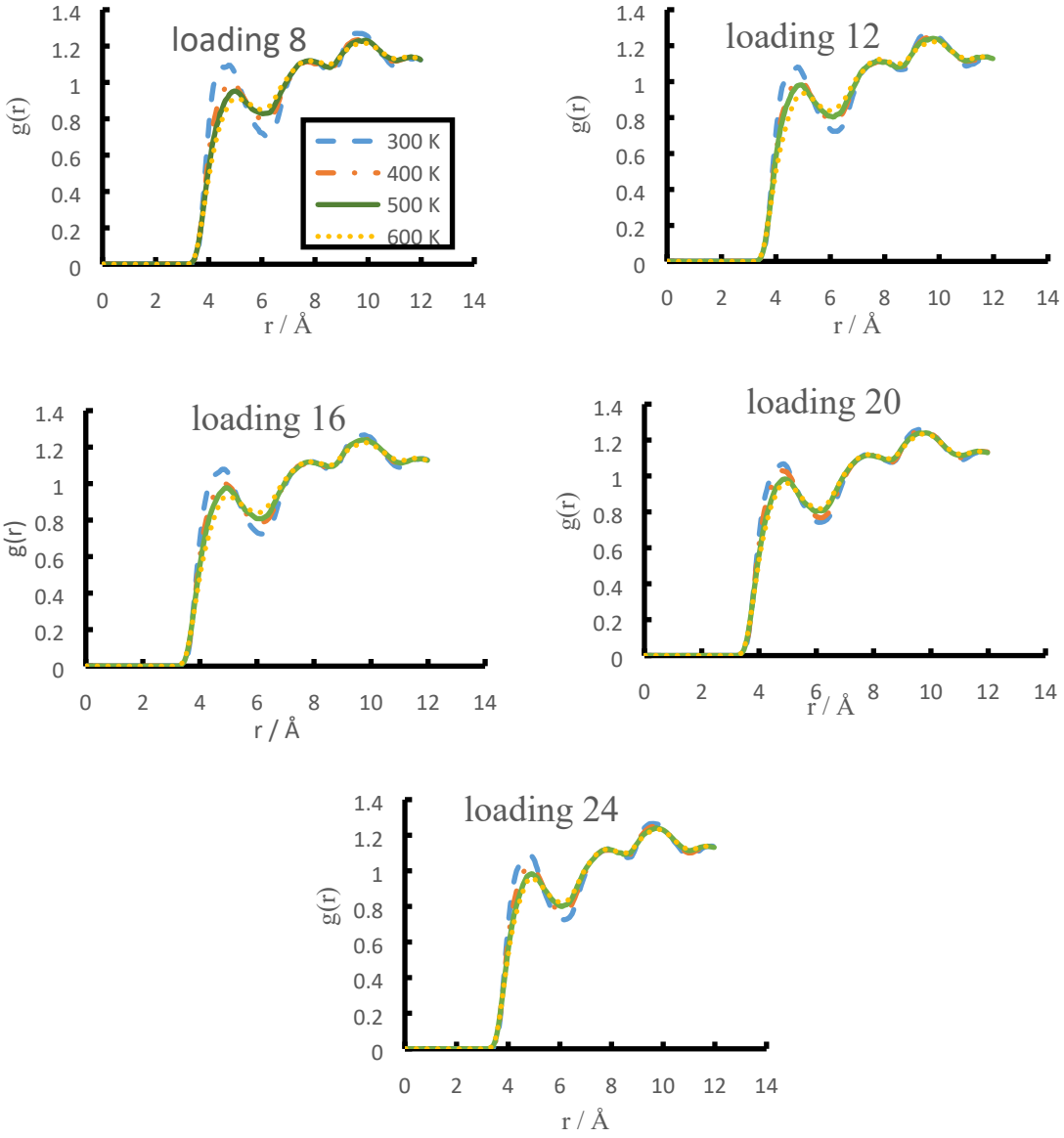

Fig. 5. The RDFs between S atom of SO_2 and Si atom of silica Y zeolite from simulations at different temperatures.

$$\beta(t) = \frac{d\log \mathrm{MSD}(t)}{d\log(t)} \tag{2}$$

where β equal to 2 represents a ballistic (free) diffusion; if β is very close to 1, it denotes a Fickian diffusion and there is a good linear regime for calculating the self-diffusion coefficient [20]. Arrhenius relation was applied to obtain the diffusion activation energy

$$D = D_0 e^{-\frac{E_{act}}{RT}} \tag{3}$$

where D_0 is pre-exponential factor and E_{act} , R, and T are the activation energy, gas constant and temperature, respectively [20,50].

VAF is defined as

$$VAF = \frac{1}{N}\sum_i \frac{v_i(t).v_i(0)}{v_i(0).v_i(0)} \tag{4}$$

where v_i introduces the velocity of particle i and N shows the number of particles [51]. In addition, RDF introduced as g_{ij} (r) is based on the following relation

$$g_{ij}(r) = \frac{\langle \Delta N_{ij}(r, r+\Delta r)\rangle V}{4\pi r^2 \Delta r N_i N_j} \tag{5}$$

where i and j refer to two species, r is the distance between two species of i and j, V is the volume of the system, $\Delta N_{ij}(r, r+\Delta r)$ denotes the ensemble-averaged number of the species j around i within a shell of Δr, and N_i and N_j are the number of i and j species [28].

The interatomic potential of mean force (PMF), $W(r)$, offers the free energy profile of the system as a function of the separation distance between the two species i and j [52,53].

$$W_{ij}(r) = -RT\ln g_{ij}(r) \tag{6}$$

3. Results and discussion

MD simulations were carried out at different temperatures and loadings for SO_2 guest molecules in fixed silica Y zeolite framework.

3.1. Dynamic properties

Fig. 2 shows the time variation of center of mass MSD of SO_2 within

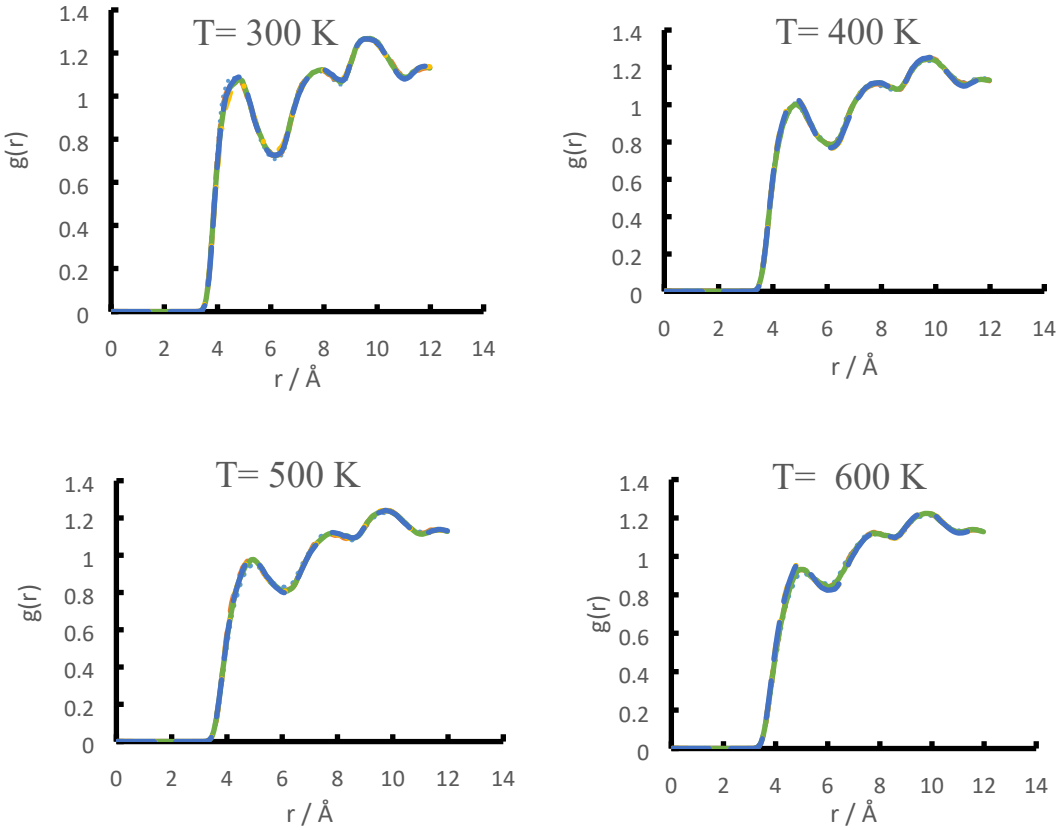

Fig. 6. The RDFs between S atom of SO_2 and Si atom of silica Y zeolite from simulations at different loadings.

the pores of silica Y zeolite for loadings 8, 12, 16, 20, and 24 SO_2 mol/u.c. at last 250 ps of simulation. The plots show a nearly linear relationship for the MSD against simulation time and a normal diffusion regime. In fact, as the temperature increases, the slope of the MSD curves increases because the kinetic energy of the guest molecules increases and allows an easier movement of the SO_2 molecules within the zeolite pores [20]; surprisingly, at loadings 16, 20, and 24 the slope of the MSD at 500 and 600 K is almost equal. Probably at higher loadings, increasing temperature could not influence the slope of MSD due to steric hindrance.

Fig. 3 represents the time variation of center of mass MSD of SO_2 calculated from the simulations at different loadings of guest molecules at studied temperatures. At 300 K, the slope of the MSD curves decreases with increasing loading. At higher loadings, steric hindrance effects and the collisions between SO_2 molecules increase; therefore, it may impede the diffusion of guest molecules and reduce the MSD [33] though at loading 24 slope is greater than loading 20. This means that at loading 20, which has the least slope of MSD, the greatest interaction of the guest molecules with the pore walls is likely, and probably all 20 molecules of SO_2 are captured in the cage. At 400 K and loadings 8, 12, and 16, the slope is almost identical meaning that there is no observed loading dependency at this temperature and loading range. But at loadings of 20 and 24, the slope is almost equal and much less than loadings of 8, 12, and 16. Again, at higher loadings, the highest interaction was observed with the pore walls. At a temperature of 500 K, the slope of MSD plot decreases with loading enhancement. As expected, the collision between SO_2 molecules prevents their diffusion into the zeolite pores. Also, the slope of the MSD curve reduces with increasing loading at 600 K although at loadings 20 and 24, the slopes are almost the same.

The linear dependence of MSD is observed with time; consequently, the self-diffusion coefficients of SO_2 in the zeolite pores were calculated from the slope of the MSD plot at last 0.25 ns by Eq. (1). Self-diffusion coefficients, β factor, and activation energies for diffusion of guest molecules in Y zeolite are presented at different temperatures and loadings in Table 2. Besides to make it more quantitative, the uncertainty values of diffusion coefficient were obtained and are reported in Table 2. These values were calculated by taking the slope at different regions (between 50 and 150, 100 and 200 and 150 and 250 ps) and then taking a mean and standard deviation. It can be seen that the trend is similar to the diffusion coefficient variation. At the considered time, β is approximately equal to one and the motion of the particle is diffusive [25]. Of course, when loading is 20, there is a slight deviation from Fickian. At higher loadings, more collisions between the adsorbate molecules and pore walls may occur. These collisions may have two effects on the diffusion of SO_2 molecules: the first is the exchange of energy, which leads to an increase in molecular diffusivity and an increase in the self-diffusion coefficient. The second effect is that the mean free path for motion in the cages reduced and the self-diffusion coefficient decreased by adsorption occupancy [54]. It seems that, here, the second effect is dominant although with increasing loading at 300, 400, and 600 K, at a loading of 20, self-diffusion coefficient passes through a minimum at intermediate coverage. This observation is in accordance with Deroche et al. [39] results. The MD results on H_2 diffusion in FAU type zeolite have shown that the diffusion coefficient increases with increasing temperature and β is approximately 1 at all loadings and temperatures [20]; therefore, Fickian diffusion was predicted. Gautam et al. [55,56] have also examined the diffusion coefficients of propane in aerogels with two points of views, experimentally and computationally by MD simulation. They have concluded that if the number of adsorbed molecules is small, all of them are immobile; however, at higher loadings, the molecules are far from the pore walls and their mobility enjoys an increase. The current observation is in accordance with Gautam et al. [55,56]. From the other side of view, it would be nice to mention that the order of SO_2 diffusion in the present study at 16 and 24 is one order greater than Sun et al. [29] observation for 4A zeolite. The difference is related to the solid structures that are different in framework topology.

According to the information in Table 2, generally, as the

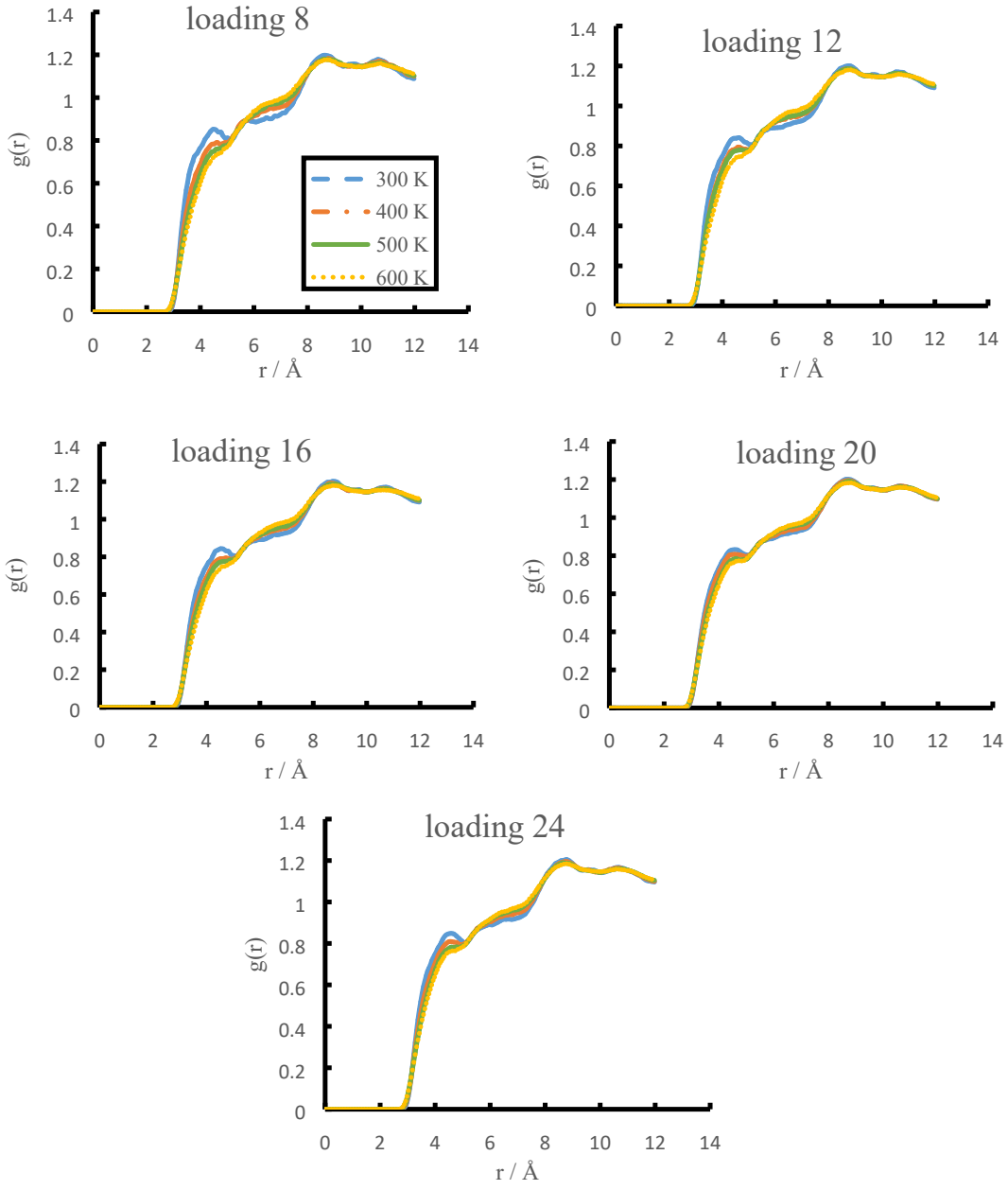

Fig. 7. The RDFs between S atom of SO_2 and O atom of silica Y zeolite from simulations at different temperatures.

temperature increases, the self-diffusion coefficient enhances because molecular movements at higher temperatures lead to more successful jump between sites. At loading 8, the temperature rising improves molecular diffusion coefficient from 9.95 $\times$ 10^{-9} $m^2.s^{-1}$ at 300 K to 34.12$\times 10^{-9}$ $m^2.s^{-1}$ at 600 K. Notice that these diffusion coefficient values are the highest in comparison to the other loadings that is related to the lowest hinderance. At the range of temperature and loading studied, the highest diffusion coefficient of SO_2 gas in silica Y zeolite is 34.12 $\times$ 10^{-9} $m^2.s^{-1}$ which is related to loading 8 and temperature 600 K. Corresponding activation energies change from 3.66 to 5.44 $kJ.mol^{-1}$. Frequently, activation energies for diffusion of SO_2 in zeolite cages show decreasing trend with increasing loading. It can be said that at the lower loading, adsorption sites are occupied by guest molecules and due to the stronger interaction of SO_2 with pore walls, the activation energy is great. Because of occupying the adsorption sites, if loading increases gradually, other SO_2 molecules diffuse into cages more easily. However, at loading 20, an increase in the energy of activation is observed instead of reduction that may demonstrate all 20 SO_2 molecules are adsorbed by zeolite. β value at loading 20 can justify the argument that at loading 20 the considerable adsorption is observed.

Fig. 4 shows the VAFs of the S atom to investigate the short time behavior of atomic movements at four temperatures for loadings 8, 12, 16, 20, and 24 mol/u.c. All VAFs are initially positive and then pass from a minimum. At all loadings, faster oscillatory behavior was observed at a temperature of 300 K. The negative sloping region observed at VAF shows backscattering of the S atoms in the zeolite cages [22,57] which is weaker with increasing temperature and the first minimum depth decreases. As the temperature rises, the minimum domain for S atom increases and the first peak becomes wider. In addition, the first peak was shifted to longer times indicating a decrease in the effect of the zeolite cage, which surrounds the SO_2 molecules. At loading 24 and $T = 300$ K, the depth of the first minimum increases, so that the negative region created at short time indicates that the molecule tolerates a strong collision with the cage.

In addition, loading dependence of the VAF of S atom can be found for temperatures of 300, 400, 500, and 600 K. With an increase of

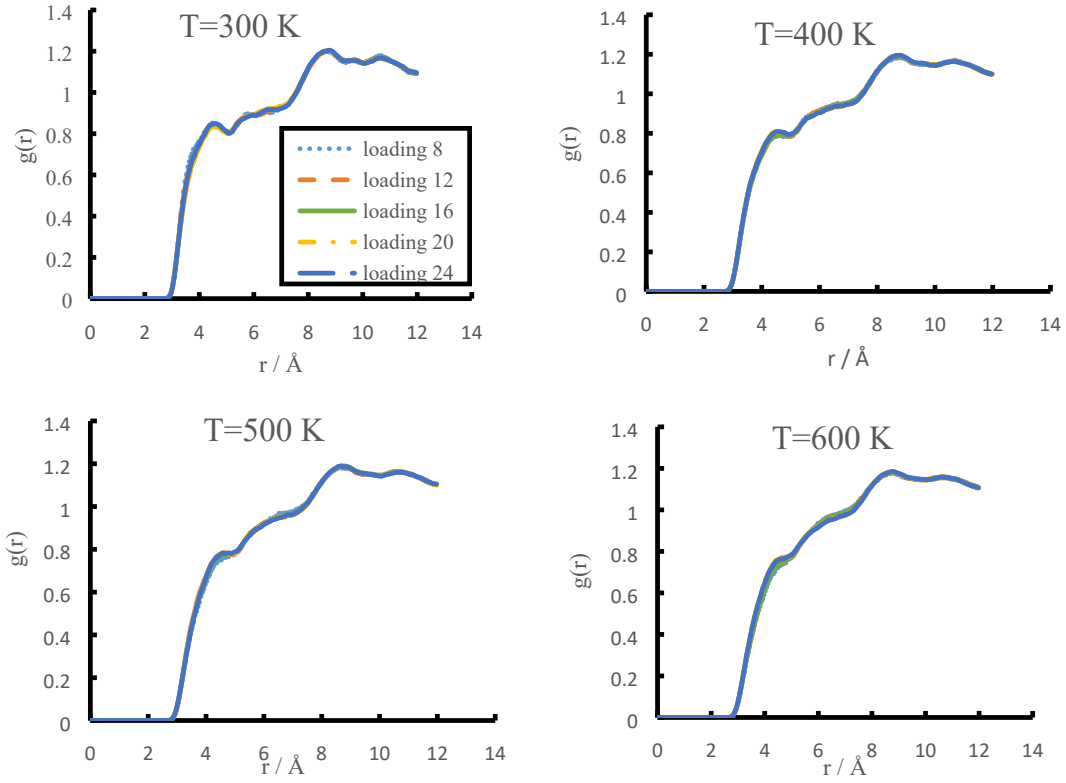

Fig. 8. The RDFs between O atom of SO_2 and O atom of silica Y zeolite from simulations at different loadings.

loading from 8 to 24, in all plots, the first minimum depth increases while the position of this minimum does not show a significant change with loading enhancement. Only at 300 K and loading 24, the first minimum is negative for S atoms while there are no negative minima in other loadings and temperatures.

3.2. Structural properties

The radial distribution function clearly determines the relative locations of the particles by calculating the probability of the presence of other particles around the desired particle. Fig. 5 displays RDFs between S atom of SO_2 molecule and Si atom of Y zeolite at loadings 8, 12, 16, 20, and 24 with the temperature varying from 300 to 600 K. As can be seen in Fig. 5, three peaks are observed in the RDF. The increase in temperature, at all loadings, decreases the intensity of the first and third peaks and spread them, but has no effect on the intensity of the second peak. Since the particle movement is slower at lower temperatures, it is easier to examine the first coordination layer [20]. For this reason, for example, at loading 8 and 300 K, the first peak is at 4.975 Å and gradually shifts to the further distances as the temperature increases. According to the distance of the first peak appearing, it can be concluded that SO_2 does not have a strong structural correlation with the zeolite Si site [20]. In addition, considering the position of the first and second peaks demonstrated that two neighboring adsorption sites are separated in zeolite at a distance of about 3 Å.

It is clearly observed in Fig. 6 that with loading variation from 8 to 24 mol/u.c., it does not possess quantifiable influence on the location of (S … Si) RDF peaks. This implies that the location of the adsorbed SO_2 molecules are preserved in its original position when new molecules coming into the zeolite, that is, the new adsorbed molecules do not have an effect on the relative location of the former molecules [28].

To deeply understand the interaction of guest gas and adsorbent, the structural correlation of SO_2 molecules with O atom of Y zeolite was also investigated. Fig. 7 displays RDFs between S atom of SO_2 molecule and O atom of Y zeolite at loadings 8, 12, 16, 20, and 24 with the temperature varying from 300 to 600 K. As can be seen, the observed peaks are not sharp that shed light on weaker interaction between guest gas with O atoms of Y zeolite. In other words, Si atom of Y zeolite plays the main role in adsorbing gas without any change in the strength of interaction with loading. Comparing Figs. 5 and 6 demonstrates that the first maximum of S…O pair interaction appears at shorter distances than S…Si; consequently, it may be concluded that this correlation provides stronger interaction. However, S…Si first peak is more intense than S…O that can be related to the greater values of ε and σ for these two atoms, Si and S. As a result, the short-range LJ interaction plays the critical role.

In addition, studying the atomistic pair correlation between O atom of gas and O atom of the Y zeolite reveals a similar trend as shown in Fig. 8. It is clear that gas ordering in the zeolite is completely due to Si atom of Y zeolite. By increasing the loading of guest gas in the adsorbent, there is no change in the position and intensity of RDFs. The effect of temperature on the structural correlation of adsorbent and adsorbate is found to be more pronounced than the effects of loading over the range of temperature and loading.

The S … S RDFs are shown at different temperatures for loadings 8 to 24 mol/u.c. in Fig. 9. At all temperatures and loadings, the RDFs are marked by the absence of the second and third peaks. The absence of the second peak in the S…S RDFs suggests that no cluster involving more than the first-shell neighbors are observed at these temperatures and adsorbate loadings investigated here. At the range of temperatures and loadings studied, the first peak is observed at 4.525 Å that is greater than the distance between gas and zeolite. This means that with increasing temperature, there is no significant shift in peak positions of S atoms. In other words, due to no clustering formation, the increase in temperature does not affect the position of SO_2 molecules relative to each other. In addition, the intensity of the RDF decreases with increasing temperature especially with an increase in temperature from 300 to 400 K due to more frequent molecular collisions.

The average number density of SO_2 found in each of a series of thin slabs was calculated from the MD simulation. Z-density profile for SO_2 at 600 K and different loadings is presented in Fig. 10. These plots all show

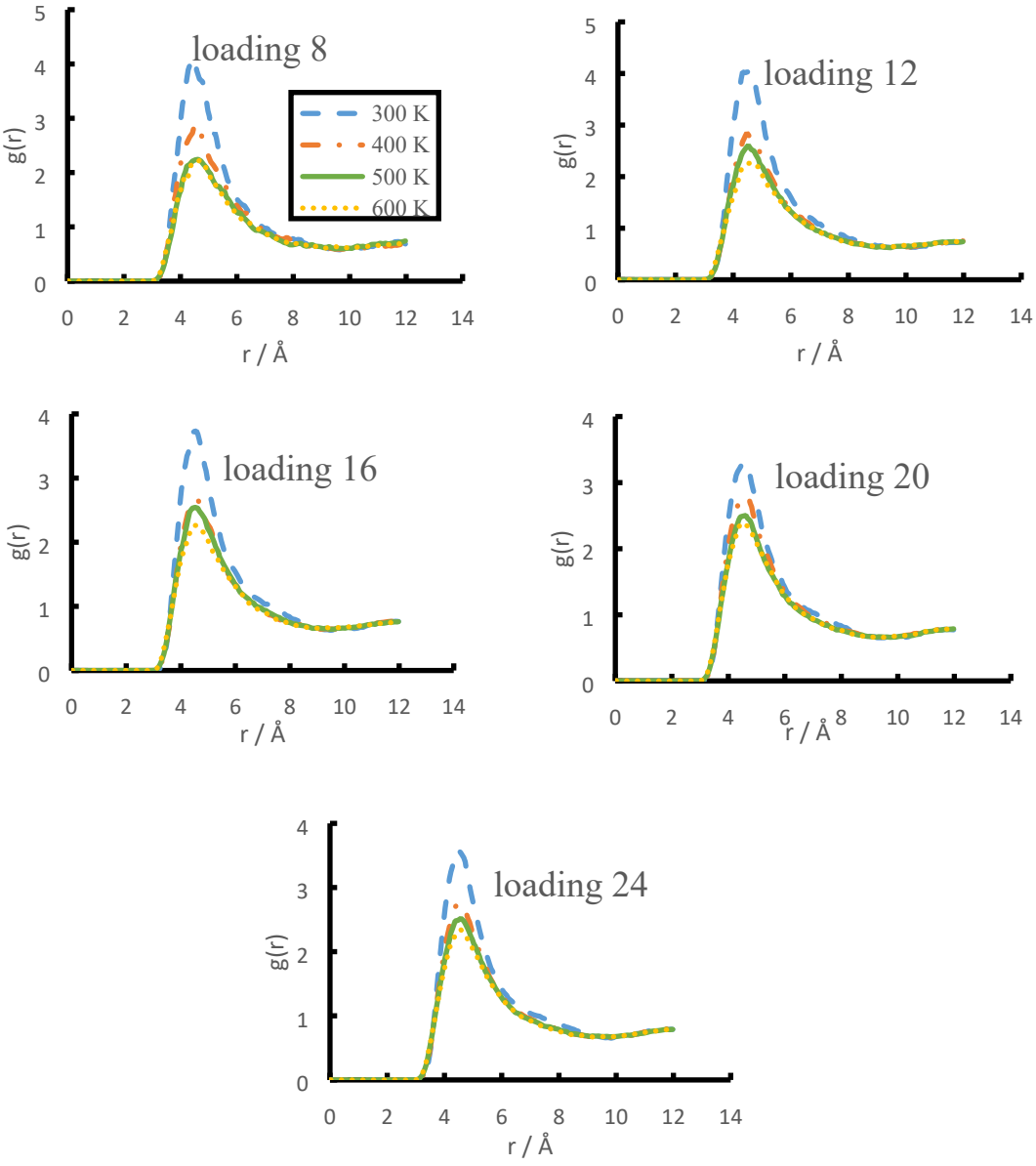

Fig. 9. The RDFs of S… S at different temperatures and loadings.

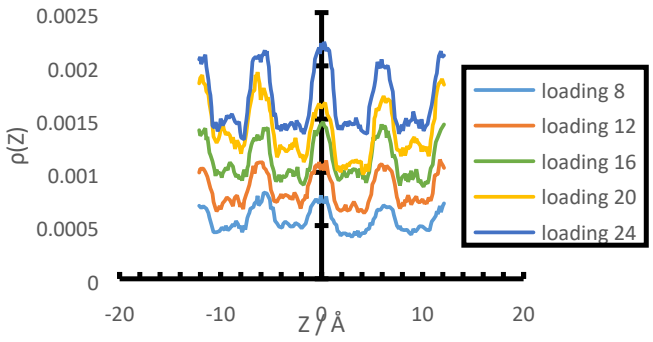

Fig. 10. Z-density profile of SO_2 gas in Y zeolite at 600 K and different loadings.

a regular progression of 5 distinct peaks at equal intervals with Z = -12, -6, 0, +6, and +12 Å. The height of these peaks is approximately the same; therefore, these Z values refer to the placement of supercages in Y zeolite. Since the zeolite structure is symmetric, the distribution of SO_2 is seen at identical and symmetrical intervals. As expected, if the loading increases, the height of the peaks increases indicating higher number of SO_2 adsorbed in the cage.

3.3. *Thermodynamic properties*

Si … S PMF plots at different loadings are shown in Fig. 11 and the temperature dependence of the PMF is investigated. The PMF plots at all temperatures and loadings have three minima. As the temperature increases, the depth of the first minimum decreases though the inverse is observed for the second and third minima. At loading 8 and temperature of 300 K, the first minimum is formed at 4.775 Å and well depth is 0.23 kJ.mol^{-1}. Additionally, with increasing temperature, the first minimum shifted to larger distance without any change in the position of the second and third minima. At temperature 300 K and at all loadings, the depth of the first minimum is said to be more energetically favorable [58]. The barrier for crossing from the second minimum to the first minimum is significant but the barrier for crossing from the third minimum to the second minimum is smaller and decreases with increasing

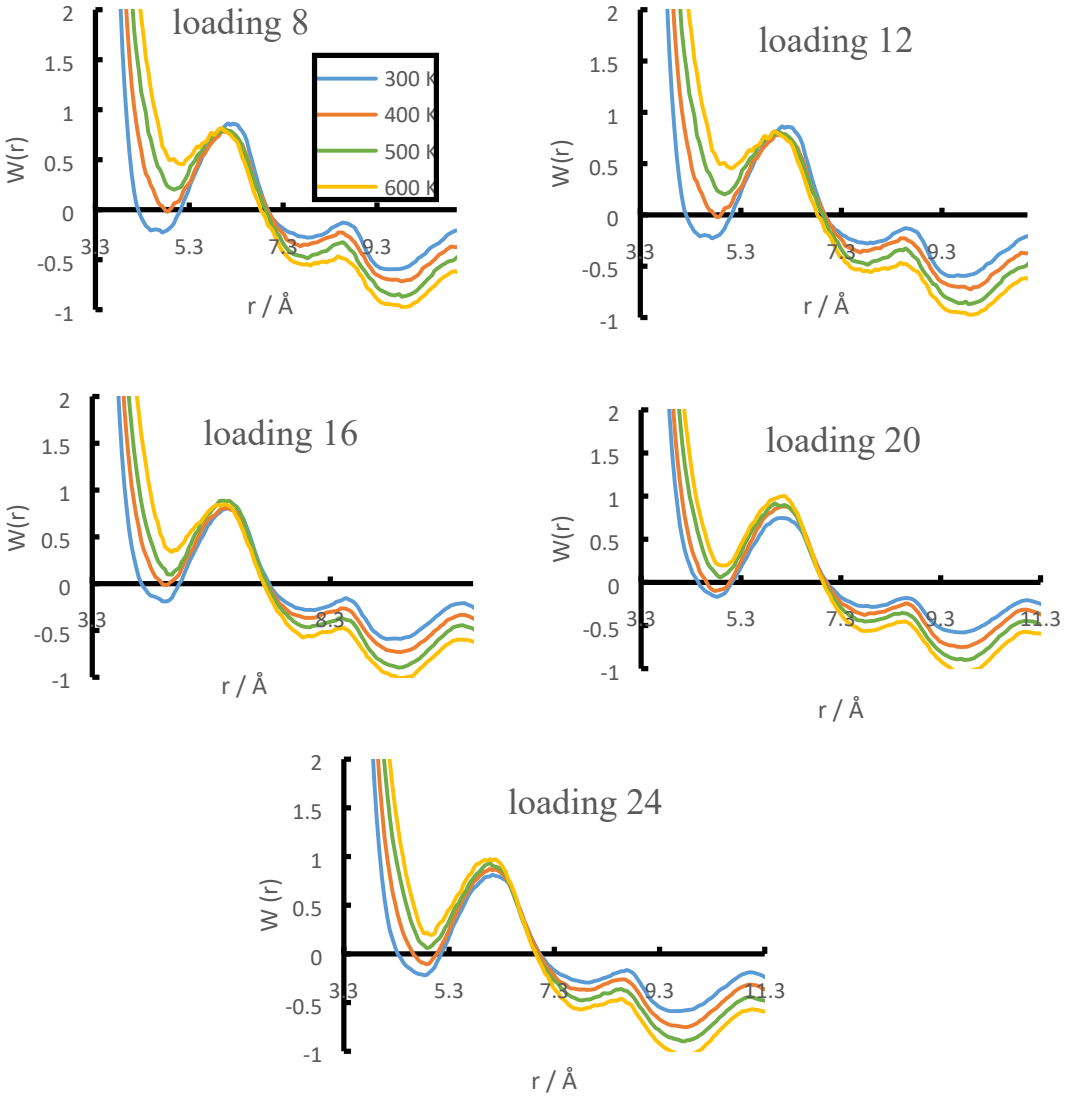

Fig. 11. PMF between S atom of SO_2 and Si atom of silica Y zeolite at different temperatures and loadings.

temperature. As can be seen, at loading 20, the difference between the depth of the first minimum in the four examined temperatures is lower than loadings 8, 12, 16, and 24. The loading dependence of the PMF was also considered. Except at temperature of 600 K, which the depth of the first minimum and the first barrier for crossing differs significantly, there is no significant difference in the PMF at other temperatures.

4. Conclusions

In the present study, it was under consideration that the temperature and loading play role in the dynamic, structure, and thermodynamic properties of SO_2 in silica Y zeolite using MD simulation. In general, the slope of the MSD plots increases with increasing temperature and decreases with increasing loading; however, at some loadings, it is the same at a temperature. It seems that the difference in loading is not great; in addition, the volume of porosity of Y zeolite is large and SO_2 molecules may diffuse into the pore without blocking their path. By calculating the β factor, it was displayed that MSD $\propto$ t, which implies the diffusion mechanism into the zeolite is Fickian. For this reason, last 250 ps of simulation was used to calculate the diffusion coefficient using Einstein's relation. Of course, at 300 K and loading 20 the lowest slope of MSD is observed and β factor shows a deviation from one; as a result, the highest adsorption of SO_2 molecules at this loading was taken place. Observation of the change trend in the diffusion coefficient shows that at each temperature, except 500 K, there is the lowest diffusion coefficient at loading 20. At each loading, except 20, the diffusion coefficient increases with temperature. As well as the activation energy, which shows a decreasing trend with increasing loading, at loading 20 this trend is violated. It has been found that the first minimum of VAF shifts toward long times with increasing temperature and there is not significant change with increasing loadings. It can be concluded that only with increasing temperature, the cage effect on SO_2 molecules lessened. Reducing the intensity of the first peak of the RDF of the center of mass of SO_2 and Si with the increase of temperature and shifting to longer distances suggests that the formation of the first layer around the central atom becomes harder. The symmetric structure of Y zeolite can be seen from the Z-density profile corresponding to the location of SO_2. From the PMF plots, it is deduced that by decreasing the temperature, the first minimum is the deepest and adsorption is favored.

CRediT authorship contribution statement

Yalda Sabahi: Data curation, Writing – original draft. **Mohammad Razmkhah:** Conceptualization, Methodology, Software. **Fatemeh Moosavi:** Visualization, Investigation, Supervision, Writing – review & editing.

Declaration of Competing Interest

The authors declare that they have no known competing financial interests or personal relationships that could have appeared to influence the work reported in this paper.

Acknowledgement

We hereby acknowledge that parts of this computation performed on the HPC center of Ferdowsi University of Mashhad. In addition, the financial support provided by Ferdowsi University of Mashhad (grant no. 3/47414) is greatly appreciated.

References

[1] M.H. Ketko, G. Kamath, J.J. Potoff, Development of an optimized intermolecular potential for sulfur dioxide, J. Phys. Chem. B 115 (17) (2011) 4949–4954.
[2] S. Yun, H. Lee, W.-E. Lee, H.S. Park, Multiscale textured, ultralight graphene monoliths for enhanced CO_2 and SO_2 adsorption capacity, Fuel 174 (2016) 36–42.
[3] I. Matito-Martos, A. Martin-Calvo, J.J. Gutiérrez-Sevillano, M. Haranczyk, M. Doblare, J.B. Parra, C.O. Ania, S. Calero, Zeolite screening for the separation of gas mixtures containing SO_2, CO_2 and CO, PCCP 16 (37) (2014) 19884–19893.
[4] L. Yin, M. Hu, D. Li, J. Chen, K. Yuan, Y. Liu, Z. Zhong, W. Xing, Multifunctional ZIF-67@SiO_2 membrane for high efficiency removal of particulate matter and toxic gases, Ind. Eng. Chem. Res. 59 (40) (2020) 17876–17884.
[5] Y. Mathieu, M. Soulard, J. Patarin, M. Molière, Mesoporous materials for the removal of SO_2 from gas streams, Fuel Process. Technol. 99 (2012) 35–42.
[6] K. Tan, S. Zuluaga, Q. Gong, Y. Gao, N. Nijem, J. Li, T. Thonhauser, Y.J. Chabal, Competitive Coadsorption of CO2 with H2O, NH3, SO2, NO, NO2, N2, O2, and CH4 in M-MOF-74 (M = Mg Co, Ni): The Role of Hydrogen Bonding, Chem. Mater. 27 (6) (2015) 2203–2217.
[7] X.-D. Song, S.e. Wang, C.e. Hao, J.-S. Qiu, Investigation of SO_2 gas adsorption in metal–organic frameworks by molecular simulation, Inorg. Chem. Commun. 46 (2014) 277–281.
[8] H. Deng, H. Yi, X. Tang, H. Liu, X. Zhou, Interactive effect for simultaneous removal of SO_2, NO, and CO_2 in flue gas on ion exchanged zeolites, Ind. Eng. Chem. Res. 52 (20) (2013) 6778–6784.
[9] M. Mohammadi, M. Foroutan, Molecular investigation of SO_2 gas absorption by ionic liquids: Effects of anion type, J. Mol. Liq. 193 (2014) 60–68.
[10] Y. Zhu, J. Gao, Y. Li, F. Sun, J. Gao, S. Wu, Y. Qin, Preparation of activated carbons for SO_2 adsorption by CO_2 and steam activation, J. Taiwan Inst. Chem. Eng. 43 (1) (2012) 112–119.
[11] F. Rahmani, D. Mowla, G. Karimi, A. Golkhar, B. Rahmatmand, SO_2 removal from simulated flue gas using various aqueous solutions: Absorption equilibria and operational data in a packed column, Sep. Purif. Technol. 153 (2015) 162–169.
[12] M.C.C. Ribeiro, Molecular Dynamics Simulation of Liquid Sulfur Dioxide, J. Phys. Chem. B 110 (17) (2006) 8789–8797.
[13] H. Yi, H. Deng, X. Tang, Q. Yu, X. Zhou, H. Liu, Adsorption equilibrium and kinetics for SO_2, NO, CO_2 on zeolites FAU and LTA, J. Hazard. Mater. 203-204 (2012) 111–117.
[14] A. Srinivasan, M.W. Grutzeck, The Adsorption of SO_2 by Zeolites Synthesized from Fly Ash, Environ. Sci. Technol. 33 (9) (1999) 1464–1469.
[15] M. Ioan-Cezar, S. I, Study of sulfur dioxide adsorption on Y zeolite, J. Serb. Chem. Soc. 69 (7) (2004) 563–569.
[16] A. Gupta, V. Gaur, N. Verma, Breakthrough analysis for adsorption of sulfur-dioxide over zeolites, Chem. Eng. Process. Process Intensif. 43 (1) (2004) 9–22.
[17] B.C. Bukowski, F.J. Keil, P.I. Ravikovitch, G. Sastre, R.Q. Snurr, M.-O. Coppens, Connecting theory and simulation with experiment for the study of diffusion in nanoporous solids, Adsorption 27 (5) (2021) 683–760.
[18] V. Van Speybroeck, K. Hemelsoet, L. Joos, M. Waroquier, R.G. Bell, C.R.A. Catlow, Advances in theory and their application within the field of zeolite chemistry, Chem. Soc. Rev. 44 (20) (2015) 7044–7111.
[19] X. Ren, R. Qu, S. Liu, H. Zhao, W. Wu, S. Hao, C. Zheng, X.-C. Wu, X. Gao, Synthesis of zeolites from coal fly ash for the removal of harmful gaseous pollutants: A review, Aerosol Air Qual. Res. 20 (2020) 1127–1144.
[20] M.H. Kowsari, S. Naderlou, Understanding the dynamics, self-diffusion, and microscopic structure of hydrogen inside the nanoporous Li-LSX zeolite, Microporous Mesoporous Mater. 240 (2017) 39–49.
[21] S. Gautam, V.K. Sharma, S. Mitra, S.L. Chaplot, R. Mukhopadhyay, Rotational dynamics of propylene in ZSM-5 zeolitic frameworks, Chem. Phys. Lett. 501 (4-6) (2011) 345–350.
[22] S. Mitra, S. Gautam, R. Mukhopadhyay, S. Sumitra, A.M. Umarji, S. Yashonath, S. L. Chaplot, Diffusion of acetylene embedded in Na–Y zeolite: QENS and MD simulation studies, Physica B 385–386 (2006) 275–278.
[23] V.K. Sharma, S. Gautam, S. Mitra, M.N. Rao, A.K. Tripathi, S.L. Chaplot, R. Mukhopadhyay, Dynamics of Adsorbed Hydrocarbon in Nanoporous Zeolite Framework, J. Phys. Chem. B 113 (23) (2009) 8066–8072.
[24] A. Buin, J. Ma, Y. Huang, S. Consta, Z. Hui, Conformational Changes of trans-1,2-Dichlorocyclohexane Adsorbed in Zeolites Studied by FT-Raman Spectroscopy and Molecular QM/MM Simulations, J. Phys. Chem. C 116 (15) (2012) 8608–8618.
[25] J.Z. Yang, Y. Chen, A.M. Zhu, Q.L. Liu, J.Y. Wu, Analyzing diffusion behaviors of methanol/water through MFI membranes by molecular simulation, J. Membr. Sci. 318 (1-2) (2008) 327–333.
[26] S. Mitra, V.K. Sharma, S.L. Chaplot, R. Mukhopadhyay, Diffusion of hydrocarbon in zeolite and effect due to pore topology: Neutron scattering and MD simulation studies, Chem. Phys. 430 (2014) 69–77.
[27] K.L. Joshi, G. Psofogiannakis, A.C.T. van Duin, S. Raman, Reactive molecular simulations of protonation of water clusters and depletion of acidity in H-ZSM-5 zeolite, PCCP 16 (34) (2014) 18433–18441.
[28] S. Dang, L. Zhao, J. Gao, C. Xu, Loading dependence of the adsorption mechanism of thiophene in FAU zeolite, Ind. Eng. Chem. Res. 55 (45) (2016) 11801–11808.
[29] Y. Sun, S. Han, Diffusion of N_2, O_2, H_2S and SO_2 in MFI and 4A zeolites by molecular dynamics simulations, Mol. Simul. 41 (13) (2015) 1095–1109.
[30] P. Santikary, S. Yashonath, G. Ananthakrishna, A molecular dynamics study of xenon sorbed in sodium Y zeolite. 1. Temperature and concentration dependence, J. Phys. Chem. 96 (25) (1992) 10469–10477.
[31] Y. Kobayashi, S. Takami, M. Kubo, A. Miyamoto, Computational chemical study on separation of benzene and cyclohexane by a NaY zeolite membrane, Desalination 147 (1-3) (2002) 339–344.
[32] P. Cosoli, M. Ferrone, S. Pricl, M. Fermeglia, Hydrogen sulphide removal from biogas by zeolite adsorption: Part I. GCMC molecular simulations, Chem. Eng. J. 145 (1) (2008) 86–92.
[33] R. Rungsirisakun, T. Nanok, M. Probst, J. Limtrakul, Adsorption and diffusion of benzene in the nanoporous catalysts FAU, ZSM-5 and MCM-22: A molecular dynamics study, J. Mol. Graph. Model. 24 (5) (2006) 373–382.
[34] J. Zhang, N. Burke, S. Zhang, K. Liu, M. Pervukhina, Thermodynamic analysis of molecular simulations of CO_2 and CH_4 adsorption in FAU zeolites, Chem. Eng. Sci. 113 (2014) 54–61.
[35] K. Mizukami, H. Takaba, Y. Kobayashi, Y. Oumi, R.V. Belosludov, S. Takami, M. Kubo, A. Miyamoto, Molecular dynamics calculations of CO_2/N_2 mixture through the NaY type zeolite membrane, J. Membr. Sci. 188 (1) (2001) 21–28.
[36] M. Kamat, W. Dang, D. Keffer, Agreement between analytical theory and molecular dynamics simulation for adsorption and diffusion in crystalline nanoporous materials, J. Phys. Chem. B 108 (1) (2004) 376–386.
[37] D.F. Plant, G. Maurin, H. Jobic, P.L. Llewellyn, Molecular dynamics simulation of the cation motion upon adsorption of CO_2 in faujasite zeolite systems, J. Phys. Chem. B 110 (29) (2006) 14372–14378.
[38] P. Demontis, H. Jobic, M.A. Gonzalez, G.B. Suffritti, Diffusion of water in zeolites NaX and NaY studied by quasi-elastic neutron scattering and computer simulation, J. Phys. Chem. C 113 (28) (2009) 12373–12379.
[39] I. Déroche, G. Maurin, B.J. Borah, S. Yashonath, H. Jobic, Diffusion of pure CH_4 and its binary mixture with CO_2 in Faujasite NaY: A combination of neutron scattering experiments and molecular dynamics simulations, J. Phys. Chem. C 114 (11) (2010) 5027–5034.
[40] H.V. Thang, L. Grajciar, P. Nachtigall, O. Bludský, C.O. Areán, E. Frýdová, R. Bulánek, Adsorption of CO_2 in FAU zeolites: Effect of zeolite composition, Catal. Today 227 (2014) 50–56.
[41] A.E.O. Lima, V.A.M. Gomes, S.M.P. Lucena, Theoretical study of CO_2:N_2 adsorption in faujasite impregnated with monoethanolamine, Braz. J. Chem. Eng. 32 (3) (2015) 663–669.
[42] M.H. Asl, F. Moosavi, J. Sargolzaei, K. Sharifi, Molecular dynamics simulation study: The decryption of bi and tri aromatics behavior with NaX zeolite, J. Mol. Graph. Model. 69 (2016) 61–71.
[43] X. Qiao, F. Zhang, F. Sha, H. Shi, J. Zhang, Solubility Properties and Absorption Mechanism Investigation of Dilute SO_2 in Propylene Glycol Monomethyl Ether + Dimethyl Sulfoxide System, J. Chem. Eng. Data 62 (6) (2017) 1756–1766.
[44] *http://www.iza-structure.org/databases/*.
[45] J.B. Nicholas, A.J. Hopfinger, F.R. Trouw, L.E. Iton, Molecular modeling of zeolite structure. 2. Structure and dynamics of silica sodalite and silicate force field, J. Am. Chem. Soc. 113 (13) (1991) 4792–4800.
[46] J.C. Palmer, J.D. Moore, T.J. Roussel, J.K. Brennan, K.E. Gubbins, Adsorptive behavior of CO_2, CH_4 and their mixtures in carbon nanospace: a molecular simulation study, PCCP 13 (9) (2011) 3985–3996.
[47] W. Smith, T.R. Forester, DL_POLY_2.0: A general-purpose parallel molecular dynamics simulation package, J. Mol. Graph. 14 (3) (1996) 136–141.
[48] H. Liu, Transport diffusivity of propane and propylene inside SWNTs from equilibrium molecular dynamics simulations, PCCP 16 (45) (2014) 24697–24703.
[49] Frerich J. Keil, Rajamani Krishna, Coppens Marc-Olivier, Modeling of diffusion in zeolites, Rev. Chem. Eng. 16 (2) (2000) 71–197.
[50] A.J. O'Malley, I. Hitchcock, M. Sarwar, I.P. Silverwood, S. Hindocha, C.R. A. Catlow, A.P.E. York, P.J. Collier, Ammonia mobility in chabazite: insight into the diffusion component of the NH_3-SCR process, PCCP 18 (26) (2016) 17159–17168.
[51] J.R. Rustad, D.A. Yuen, F.J. Spera, The sensitivity of physical and spectral properties of silica glass to variations of interatomic potentials under high pressure, Phys. Earth Planet. Inter. 65 (3-5) (1991) 210–230.
[52] E. Iskrenova-Tchoukova, A.G. Kalinichev, R.J. Kirkpatrick, Metal Cation Complexation with Natural Organic Matter in Aqueous Solutions: Molecular Dynamics Simulations and Potentials of Mean Force, Langmuir 26 (20) (2010) 15909–15919.
[53] J. Van Eerden, W.J. Briels, S. Harkema, D. Feil, Potential of mean force by thermodynamic integration: Molecular-dynamics simulation of decomplexation, Chem. Phys. Lett. 164 (4) (1989) 370–376.
[54] F. Jianfen, W. Qiuxia, G. Xuedong, X. Heming, Concentration dependence of ethene diffusion in H[Al]ZSM-5 studied by molecular dynamics, J. Mol. Struct. (Thoechem) 638 (1-3) (2003) 129–134.

[55] S. Gautam, T. Le, A. Striolo, D. Cole, Molecular dynamics simulations of propane in slit shaped silica nano-pores: direct comparison with quasielastic neutron scattering experiments, PCCP 19 (48) (2017) 32320–32332.
[56] S. Gautam, T. Liu, G. Rother, N. Jalarvo, E. Mamontov, S. Welch, J. Sheets, M. Droege, D.R. Cole, Dynamics of propane in nanoporous silica aerogel: A quasielastic neutron scattering study, J. Phys. Chem. C 119 (32) (2015) 18188–18195.
[57] S. Balasubramanian, K.J. Rao, Molecular dynamics investigation of structure and transport in the K_2O–$2SiO_2$ system using a partial charge based model potential, J. Phys. Chem. C 98 (42) (1994) 10871–10880.
[58] M. Forsyth, V.A. Payne, M.A. Ratner, S.W. de Leeuw, D.F. Shriver, Molecular dynamics simulations of highly concentrated salt solutions: Structural and transport effects in polymer electrolytes, Solid State Ionics 53-56 (1992) 1011–1026.